J. Fluid Mech. (1998), *vol.* 368, *pp.* 359–375. Printed in the United Kingdom

Electrohydrodynamic deformation and interaction of drop pairs

By J. C. BAYGENTS[1], N. J. RIVETTE[1] AND H. A. STONE[2]

[1] Department of Chemical and Environmental Engineering, University of Arizona, Tucson, AZ 85721, USA

[2] Division of Engineering and Applied Sciences, Harvard University, Cambridge, MA 02138, USA

(Received 8 September 1996 and in revised form 30 March 1998)

The motion of two drops in a uniform electric field is considered using the leaky dielectric model. The drops are assumed to have no native charge and a dielectrophoretic effect favours translation of the drops toward one another. However, circulatory flows that stem from electrohydrodynamic stresses may either act with or against this dielectrophoretic effect. Consequently, both prolate and oblate drop deformations may be generated and significant deformation occurs near drop contact owing to enhancement of the local electric field. For sufficiently widely spaced drops, electrohydrodynamic flows dominate direct electrical interactions so drops may be pushed apart, though closely spaced drops almost always move together as a result of the electrical interaction or deformation.

1. Introduction

Externally applied electric fields provide a well-known means for manipulating suspensions of drops and bubbles (Arp, Foister & Mason 1980). Common applications span a variety of multiphase flows (Byers & Amarnath 1995), including enhanced coalescence, emulsion breaking and demixing operations for dispersions (Ptasinski & Kerkhof 1992), electrophoretic migration of charged drops (Baygents & Saville 1991*a*,*b*), enhanced heat and mass transfer owing to electroconvection (e.g. Scott 1989), electrospraying (Harris & Basaran 1993) and aqueous two-phase partitioning (Brooks *et al.* 1984). A fundamental understanding of the microstructural response of these processes may be sought by describing the fluid motion for isolated drops and drop pairs exposed to electric fields. The former subject has been well-studied, but there is a dearth of information regarding the behaviour of drop pairs in viscous liquids exposed to electric fields. In this paper we report an investigation of this latter subject, treating in particular drop deformation and hydrodynamic interactions.

A seminal contribution to the understanding of the behaviour of isolated emulsion drops in electric fields was made by Taylor (1966). Motivated by the experiments of Allan & Mason (1962), Taylor demonstrated that conductive processes play an important role in determining how a drop, which is dispersed in another liquid, deforms in response to the imposed field. Taylor's analysis was predicated on a model which has since come to be known as the *leaky dielectric*. Taylor argued that real dielectric liquids were not perfect (a perfect dielectric being one which passed no current) insofar as they would conduct a small amount of electrical current (for example, owing to the presence of ions in solution). Subsequent investigations

have confirmed the essential premise that conduction processes cannot be altogether ignored, and have shown the leaky dielectric to be a useful quantitative and conceptual model (Torza, Cox & Mason 1971; Baygents & Saville 1989; Vizika & Saville 1992).

Drop deformation in these systems depends on the electrical properties of the fluid. If the fluids are treated as perfect dielectrics, then the electrical stresses act only normal to the interface, an isolated drop deforms into a prolate spheroidal shape, and the final equilibrium state is one with no fluid motion. Accounting for conduction processes according to the leaky dielectric model shows that tangential electrical stresses act at the drop surface and drive steady circulation in and about a fluid body. Viscous stresses generated by the flow are now capable of producing both prolate and oblate drop distortions. Furthermore, these circulation patterns have been recognized to be of practical consequence inasmuch as they may lead to enhanced heat and mass transfer and, as a result of the associated viscous stresses, drop deformation occurs. As our presentation unfolds, it will become evident that the circulation patterns also play a substantive role in the pairwise response of emulsion drops: the hydrodynamic interactions that occur owing to the circulations can be significant and even dominate the direct electrical interactions between the pair.

There have been several investigations on the effect of a uniform electric field on two neighbouring drops, though most studies invoke approximations more suited to the description of aerosols rather than emulsions. For example, Brazier-Smith (1971) and Brazier-Smith, Jennings & Latham (1971) considered the finite deformation of highly conductive (water) drops but neglected viscous effects. Their work was stimulated by that of Taylor (1968) and Latham & Roxburgh (1966) on drops and bubbles dispersed in air, which is essentially a non-conducting medium. Specifically, Taylor studied the coalescence of closely spaced soap bubbles held in place by a ring device, as well as the coalescence of water drops held at the ends of hypodermic needles, while Latham & Roxburgh studied adjacent water drops supported on Teflon rods. Taken together, these studies illustrated the significant role played by *electrical* interactions between the drops. Nevertheless, for the systems investigated, viscous hydrodynamic interactions played at most a subordinate role.

The case of viscous interactions between drop pairs has been has been investigated recently by Zhang, Basaran & Wham (1995), who used a population dynamics approach to model electrically enhanced drop collision and coalescence in emulsions. The analysis of Zhang *et al.* is noteworthy because, among other reasons, it provides a framework for characterizing the increased coalescence rate owing to an applied electric field. However, the types of emulsions studied – perfectly conducting drops dispersed in a perfect dielectric liquid – do not involve the sort of coupling of the electric field and the viscous flow that is present in leaky dielectric systems. Thus, the electrically driven circulations, first elucidated by Taylor (for an isolated drop), are absent.

Use of the leaky dielectric model to analyse the two-drop problem has been made previously by Sozou (1975), who examined the situation in the limit that drop deformation was negligible and that there was no relative motion of the drops. These two stipulations left unanswered several fundamental questions regarding the electrically driven, temporal evolution of the microstructure of an emulsion. For example, what is the role of deformation in bringing the drop surfaces into close proximity, and what is the relative motion of the drops? Here we address the basic two-drop problem using integral equation methods to follow the changing drop shapes and the relative motion of the drops. The numerical study is nevertheless restricted to an axisymmetric geometry and drops of equal sizes, as was the analytical study of

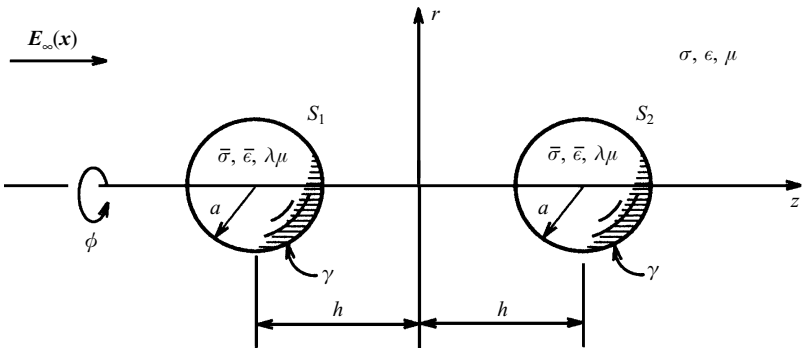

FIGURE 1. Axisymmetric two-drop problem with an electric field aligned with the line of centres.

Sozou (1975). The use of the integral equation representations for both the electric field and the viscous flow follows in the spirit of Sherwood (1988) who analysed the low-Reynolds-number deformation of an isolated drop in an electric field. An analysis of the deformation of a perfect dielectric drop for the limit of slender shapes was given by Sherwood (1991) and for conically tipped drops by Li, Halsey & Lobkovsky (1994); see also Stone, Lister & Brenner (1998).

We begin in §§ 2.1 and 2.2 with a complete description of the equations governing the electric field, the viscous flow, and the boundary conditions which couple the electrical stresses to the flow. Analytical results for isolated spherical drops in uniform electric fields are summarized in § 2.3 since the solutions prove useful for characterizing the response of the two-drop problem. Integral equation representations for the electric and velocity fields, and a brief description of the numerical implementation in this free-boundary problem, are given in § 2.4 and § 2.5, respectively. After first summarizing some simple scaling arguments in § 3.1, numerical results for perfect dielectric drop pairs are presented in § 3.2 and conduction processes, studied within the leaky dielectric model, are examined in § 3.3.

2. Governing equations

Consider two equal-size, uncharged drops with identical material properties. The drops have undeformed radius a, viscosity $\lambda\mu$, dielectric constant $\bar{\epsilon}$ and electrical conductivity $\bar{\sigma}$, and are suspended in a Newtonian fluid with corresponding properties μ, ϵ and σ, respectively. The interfacial tension is denoted γ and is assumed to be constant and independent of the electric field. An electric field $\boldsymbol{E}_\infty$, uniform at large distance, is applied parallel to the line of centres of the drops (see figure 1). Electric (Maxwell) stresses produce deformation of the drops and also drive fluid motions, the strength and character of which depend substantially on whether the fluids behave as perfect ($\sigma = \bar{\sigma} = 0$) or leaky dielectrics. Both electrical interactions and fluid flow produce translation of the drops, which is coupled to shape distortions that occur owing to electrical and viscous stresses. In this section we summarize the basic equations for electrohydrodynamic investigations based upon Taylor's leaky dielectric model.

2.1. *The electric field*

Taylor introduced the leaky dielectric model to account for the presence of (possibly weak) conduction processes in common dielectric fluids owing to the inevitable

presence of ions. Typically the propagation time of electromagnetic waves is very fast compared to the times characteristic of the electrohydrodynamic motions (Melcher 1973) and thus, for times longer than the charge relaxation time $\epsilon\epsilon_0/\sigma$, which is typically less than a second, any free charge is confined to the interfacial region. It follows that the electric field in the two fluid phases is irrotational ($\nabla \wedge \boldsymbol{E} = \boldsymbol{0}, \boldsymbol{E} = -\nabla\phi$) and so according to Gauss' law

$$\nabla \cdot \boldsymbol{E} = 0 \quad \text{or} \quad \nabla^2\phi = 0 \quad \text{for} \quad \boldsymbol{x} \in V, \tag{1a}$$

$$\nabla \cdot \bar{\boldsymbol{E}} = 0 \quad \text{or} \quad \nabla^2\bar{\phi} = 0 \quad \text{for} \quad \boldsymbol{x} \in \bar{V}. \tag{1b}$$

The boundary conditions at the fluid–fluid interfaces S_1 and S_2 are

$$\boldsymbol{n} \cdot \boldsymbol{E} = \frac{\bar{\sigma}}{\sigma}\boldsymbol{n} \cdot \bar{\boldsymbol{E}} \quad \text{and} \quad \boldsymbol{t} \cdot \boldsymbol{E} = \boldsymbol{t} \cdot \bar{\boldsymbol{E}} \quad \text{for} \quad \boldsymbol{x}_s \in S_i \quad (i = 1, 2), \tag{2a}$$

$$\boldsymbol{E} \to \boldsymbol{E}_\infty \quad \text{as} \quad |\boldsymbol{x}| \to \infty. \tag{2b}$$

Here $\boldsymbol{x}$ is the position vector, $\boldsymbol{x}_s$ is a position vector to a point along the fluid–fluid interface, V is the domain of the suspending fluid, $\bar{V}$ the drop fluid, and $\boldsymbol{n}$ and $\boldsymbol{t}$ are the unit normal and tangent vectors at the interface (see figure 1). When both phases are perfect dielectrics the dielectric constant ratio $\bar{\epsilon}/\epsilon$ replaces the conductivity ratio in (2*a*).

The discontinuity in electrical properties at the drop–suspending fluid interface causes a jump in the Maxwell stress tensor $\boldsymbol{T}^E$:

$$\boldsymbol{T}^E = \epsilon\epsilon_0 \left(\boldsymbol{E}\boldsymbol{E} - \tfrac{1}{2}E^2\boldsymbol{I}\right). \tag{3}$$

The corresponding jump in the electrical stress across the fluid–fluid interface is ($[\![\ ]\!] \equiv$ 'external' - 'internal')

$$[\![\boldsymbol{n} \cdot \boldsymbol{T}^E]\!] = \epsilon\epsilon_0 \left\{ \frac{1}{2}\left[E_n^2\left(1 - \frac{\bar{\epsilon}/\epsilon}{(\bar{\sigma}/\sigma)^2}\right) - E_t^2\left(1 - \frac{\bar{\epsilon}}{\epsilon}\right)\right]\boldsymbol{n} + E_t E_n\left(1 - \frac{\bar{\epsilon}/\epsilon}{\bar{\sigma}/\sigma}\right)\boldsymbol{t}\right\}, \tag{4}$$

where $E_n = \boldsymbol{n} \cdot \boldsymbol{E}$ and $E_t = \boldsymbol{t} \cdot \boldsymbol{E}$ denote, respectively, the normal and tangential components of the electric field evaluated just outside the drop surface. In the absence of an applied flow field, the Maxwell stresses are responsible for fluid motion and drop deformation. We note that for a perfect dielectric, it is consistent to replace $\bar{\sigma}/\sigma$ by $\bar{\epsilon}/\epsilon$ and in this case the interfacial stress jump is purely normal to the interface (and so drives no steady fluid motion in isolated drops), with the value

$$[\![\boldsymbol{n} \cdot \boldsymbol{T}^E]\!]_{\substack{\text{perfect} \\ \text{dielectric}}} = \tfrac{1}{2}\epsilon\epsilon_0\left(E_n^2 + \frac{\bar{\epsilon}}{\epsilon}E_t^2\right)\left(1 - \frac{\epsilon}{\bar{\epsilon}}\right)\boldsymbol{n}. \tag{5}$$

2.2. *Electrohydrodynamic fluid motion at low Reynolds numbers; non-dimensionalization*

Assuming the Reynolds number is small and gravitational influences may be neglected, the velocity, pressure, and stress fields ($\boldsymbol{u}, p, \boldsymbol{T}^N$) in each Newtonian fluid phase obey

$$\mu\nabla^2\boldsymbol{u} - \nabla p = \nabla \cdot \boldsymbol{T}^N = \boldsymbol{0} \quad \text{where} \quad \boldsymbol{T}^N = -p\boldsymbol{I} + \mu\left(\nabla\boldsymbol{u} + (\nabla\boldsymbol{u})^T\right). \tag{6}$$

The velocity is continuous across the interface, $\boldsymbol{u} = \bar{\boldsymbol{u}}$ for $\boldsymbol{x}_s \in S_i$, and at the interface the jump in the total stress (viscous plus electric) is balanced by the interfacial tension:

$$[\![\boldsymbol{n} \cdot \boldsymbol{T}^N + \boldsymbol{n} \cdot \boldsymbol{T}^E]\!] = \gamma\boldsymbol{n}\nabla_s \cdot \boldsymbol{n}. \tag{7}$$

Here $\nabla_s \equiv (\boldsymbol{I} - \boldsymbol{n}\boldsymbol{n}) \cdot \nabla$ is the surface gradient operator and $\nabla_s \cdot \boldsymbol{n}$ is the mean curvature of the interface.

It follows from the boundary conditions that electrohydrodynamic viscous flows have typical velocities $u = O(\epsilon\epsilon_0 E_\infty^2 a/\mu)$. Thus, in the analysis and simulations given in the remainder of the paper, electric fields, velocities, and times are scaled by $E_\infty, u, a/u$, while the pressure and stress fields in the exterior and drop fluids are scaled, respectively, by $\mu u/a$ and $\lambda\mu u/a$. Also, viscous stresses cause drop deformation, whose magnitude typically depends on the interfacial tension, and is characterized by the electric capillary number $\mathscr{C}_e$:

$$\mathscr{C}_e = \frac{\epsilon\epsilon_0 E_\infty^2 a}{\gamma}. \tag{8}$$

The two-drop electrodynamic problem may then be characterized completely by specifying the dimensionless parameters $\bar{\epsilon}/\epsilon, \bar{\sigma}/\sigma, \lambda$ and $\mathscr{C}_e$. The (dimensional) initial separation of the centres of mass of the two initially spherical drops is denoted $2h$. We note that the low-Reynolds-number approximation upon which the hydrodynamic analysis is based requires that $\mathscr{R} = \rho\epsilon\epsilon_0 E_\infty^2 a^2/\mu^2 \ll 1$. At small inter-drop separations the above estimates are not expected to be so representative since the neighbouring second drop enhances the local electric field. As a final remark, we note that boundary condition (2*a*) requires that the electric Reynolds number, $\mathscr{R}_{el} = \epsilon^2\epsilon_0^2 E_\infty^2/\mu\sigma$, which represents the ratio of the charge relaxation time $\epsilon\epsilon_0/\sigma$ to the typical convection time $a/u = \mu/\epsilon\epsilon_0 E_\infty^2$ in the fluid, must be small, and this is consistent with many (though not all) experiments (e.g. Torza *et al.* 1971; Vizika & Saville 1992). In our numerical work we have studied a wide range of electrical property values, $10^{-1} < \bar{\epsilon}/\epsilon < 100$ and $10^{-2} < \bar{\sigma}/\sigma < 10^2$ (e.g. see figure 7) and such values span the range investigated experimentally (Allan & Mason 1962; Torza *et al.* 1971; Vizika & Saville 1992).

2.3. *An isolated spherical drop in a uniform electric field*

The shape and fluid motion of an isolated nearly spherical drop in a uniform electric field is a classical problem in electrohydrodynamics. This simple solution is useful for understanding several qualitative and quantitative features of the electrical and hydrodynamic responses of the two-drop system.

The dimensionless electric fields external and internal to an isolated spherical conducting drop are

$$\boldsymbol{E}(\boldsymbol{r}) = \boldsymbol{E}_\infty + \frac{(\bar{\sigma}/\sigma - 1)}{(\bar{\sigma}/\sigma + 2)}\left[\frac{3\boldsymbol{E}_\infty \cdot \boldsymbol{r}\boldsymbol{r}}{r^5} - \frac{\boldsymbol{E}_\infty}{r^3}\right], \tag{9a}$$

$$\bar{\boldsymbol{E}}(\boldsymbol{r}) = \frac{3}{(\bar{\sigma}/\sigma + 2)}\boldsymbol{E}_\infty \quad \text{(a uniform field)}, \tag{9b}$$

where $\boldsymbol{r}$ is the position vector measured from the drop centre.

The electric field gives rise to a dimensionless tangential interfacial electric stress (equation (4))

$$\boldsymbol{t} \cdot [\![\boldsymbol{n} \cdot \boldsymbol{T}^E]\!] = \frac{9\,(\bar{\sigma}/\sigma - \bar{\epsilon}/\epsilon)}{(\bar{\sigma}/\sigma + 2)^2}\,(\boldsymbol{E}_\infty \cdot \boldsymbol{t})\,(\boldsymbol{E}_\infty \cdot \boldsymbol{n}), \tag{10}$$

which drives fluid motion. The external and internal velocity fields, scaled by $\epsilon\epsilon_0 E_\infty^2 a/\mu$, are, respectively (note: $\boldsymbol{E}_\infty \cdot \boldsymbol{E}_\infty = 1$),

$$\boldsymbol{u}(\boldsymbol{r}) = \frac{9}{5(1+\lambda)}\frac{(\bar{\sigma}/\sigma - \bar{\epsilon}/\epsilon)}{(\bar{\sigma}/\sigma + 2)^2}\left\{r^{-5}(\boldsymbol{E}_\infty \cdot \boldsymbol{r})\boldsymbol{E}_\infty + \tfrac{3}{2}\left(r^{-5} - \tfrac{5}{3}r^{-7}\right)(\boldsymbol{E}_\infty \cdot \boldsymbol{r})^2\boldsymbol{r} - \tfrac{1}{2}\left(r^{-3} - \tfrac{5}{3}r^{-5}\right)(\boldsymbol{E}_\infty \cdot \boldsymbol{E}_\infty)\boldsymbol{r}\right\}, \tag{11a}$$

$$\bar{\boldsymbol{u}}(\boldsymbol{r}) = -\frac{9}{5(1+\lambda)}\frac{\left(\bar{\sigma}/\sigma - \bar{\epsilon}/\epsilon\right)}{\left(\bar{\sigma}/\sigma + 2\right)^2}\left\{\tfrac{3}{2}\left(1 - \tfrac{5}{3}r^2\right)(\boldsymbol{E}_\infty \cdot \boldsymbol{r})\boldsymbol{E}_\infty + (\boldsymbol{E}_\infty \cdot \boldsymbol{r})^2\boldsymbol{r} - \tfrac{1}{2}\left(1 - r^2\right)(\boldsymbol{E}_\infty \cdot \boldsymbol{E}_\infty)\boldsymbol{r}\right\}. \quad (11b)$$

One important physical feature may be deduced from this solution. In spherical coordinates, the velocity tangent to the surface is

$$u_\theta(r = a, \theta) = -\frac{9\left(\bar{\sigma}/\sigma - \bar{\epsilon}/\epsilon\right)}{5\left(1+\lambda\right)\left(\bar{\sigma}/\sigma + 2\right)^2}\cos\theta\sin\theta, \quad (12)$$

where θ, measured from the positive z-axis, is the angle between the imposed field $\boldsymbol{E}_\infty$ and the position vector $\boldsymbol{r}$. Thus, from (10) or (12), we observe that the sign of $(\bar{\sigma}/\sigma - \bar{\epsilon}/\epsilon)$ determines the sense of the convection. External convection generates viscous stresses that favour formation of prolate shapes for $\bar{\epsilon}/\epsilon < \bar{\sigma}/\sigma$ and oblate shapes for $\bar{\epsilon}/\epsilon > \bar{\sigma}/\sigma$, though the detailed shape of the drop is influenced by electrical stresses too (see equation (14) below).

The corresponding drop deformation D was originally calculated by Taylor (1966) and has the form (Torza *et al.* 1971)

$$D = \frac{L-B}{L+B} = \frac{9\mathscr{C}_e}{16}\frac{f_d\left(\bar{\sigma}/\sigma, \bar{\epsilon}/\epsilon, \lambda\right)}{\left(2 + \bar{\sigma}/\sigma\right)^2}, \quad (13)$$

where

$$f_d\left(\frac{\bar{\sigma}}{\sigma}, \frac{\bar{\epsilon}}{\epsilon}, \lambda\right) = \left(\frac{\bar{\sigma}}{\sigma}\right)^2 + 1 - 2\frac{\bar{\epsilon}}{\epsilon} + \frac{3}{5}\left(\frac{\bar{\sigma}}{\sigma} - \frac{\bar{\epsilon}}{\epsilon}\right)\frac{(2+3\lambda)}{(1+\lambda)}. \quad (14)$$

Here L is the end-to-end length of the drop measured along the axis of symmetry and B is the maximum breadth in the transverse direction. By convention, $f_d > 0, = 0$, or < 0 correspond to prolate, spherical or oblate shapes, respectively. For perfect dielectrics, equation (14) shows that the shapes are always prolate. Also, f_d is only a weak function of λ. Note that D depends on $\mathscr{C}_e$ and f_d, so that deformations may possibly be small even when $\mathscr{C}_e = O(1)$.

2.4. *Integral equation representations for the velocity and electric fields*

The form of the governing equations allows integral equation representations to be developed for both the electric and velocity fields internal and external to the drop (Sherwood 1988), and these equations are particularly useful for the multiple drops and non-spherical shapes that are of interest here. In particular, it is straightforward to use the usual integral equation solution for the electric potential ϕ to derive an integral equation for the electric field. Since the tangential component of the electric field is continuous at the interface while the normal component undergoes a jump whenever the drop and suspending fluid have different electrical properties, we find

$$\boldsymbol{E}_\infty(\boldsymbol{x}) + \frac{\left(\bar{\sigma}/\sigma - 1\right)}{4\pi\bar{\sigma}/\sigma}\int_{S_i}\frac{(\boldsymbol{x}-\boldsymbol{y})}{|\boldsymbol{x}-\boldsymbol{y}|^3}E_n(\boldsymbol{y})\,\mathrm{d}S_y = \begin{cases}\boldsymbol{E}(\boldsymbol{x}), & \boldsymbol{x} \in V, \quad (15a)\\ \tfrac{1}{2}\left[\boldsymbol{E}(\boldsymbol{x}) + \bar{\boldsymbol{E}}(\boldsymbol{x})\right], & \boldsymbol{x}_s \in S_i = S_1 + S_2, \quad (15b)\\ \bar{\boldsymbol{E}}(\boldsymbol{x}), & \boldsymbol{x} \in \bar{V}, \quad (15c)\end{cases}$$

where $\boldsymbol{E}_\infty$ is the external electric field (not necessarily uniform). The unknown normal component of the electric field (evaluated from the continuous phase) for points on the boundary, $E_n(\boldsymbol{x}_s)$, may be determined by solving an integral equation of the second kind, which is obtained by taking the inner product of equation (15) with $\boldsymbol{n}(\boldsymbol{x}_s)$ at

points $\boldsymbol{x}_s$ along the interface and using boundary condition (2*a*):

$$E_n(\boldsymbol{x}_s) = \frac{2\bar{\sigma}/\sigma}{1+\bar{\sigma}/\sigma}\boldsymbol{n}(\boldsymbol{x}_s)\cdot\boldsymbol{E}_\infty(\boldsymbol{x}_s) + \frac{(\bar{\sigma}/\sigma - 1)}{2\pi\,(\bar{\sigma}/\sigma + 1)}\boldsymbol{n}(\boldsymbol{x}_s)\cdot\int_{S_i}\frac{(\boldsymbol{x}_s-\boldsymbol{y})}{|\boldsymbol{x}_s-\boldsymbol{y}|^3}E_n(\boldsymbol{y})\,\mathrm{d}S_y. \quad (16)$$

Equation (16) determines the distribution of $E_n(\boldsymbol{x}_s)$ as a function of the conductivity ratio and the drop shapes S_i. Once $E_n(\boldsymbol{x}_s)$ is known, the tangential component, $\boldsymbol{t}\cdot\boldsymbol{E} = E_t$, of the electric field is obtained by an integration of (15). Related integral equation treatments for this problem have been given, for example, by Miksis (1981).

Integral equation methods for determining the velocity field in Stokes flows are also now standard. In the case that there is no imposed flow at large distances, the velocity in a two-phase Stokes flow follows from an integral representation (Rallison & Acrivos 1978, Pozrikidis 1992; Tanzosh, Manga & Stone 1992)

$$-\frac{1}{\mu}\int_{S_i}[\![\boldsymbol{n}\cdot\boldsymbol{T}^N]\!]\cdot\boldsymbol{J}\,\mathrm{d}S_y - (1-\lambda)\int_{S_i}\boldsymbol{n}\cdot\boldsymbol{K}\cdot\boldsymbol{u}\,\mathrm{d}S_y = \begin{cases}\boldsymbol{u}(\boldsymbol{x}), & \boldsymbol{x}\in V, \quad (17a)\\ \dfrac{(1+\lambda)}{2}\boldsymbol{u}(\boldsymbol{x}_s), & \boldsymbol{x}_s\in S_i, \quad (17b)\\ \lambda\bar{\boldsymbol{u}}(\boldsymbol{x}), & \boldsymbol{x}\in\bar{V}, \quad (17c)\end{cases}$$

where the jump in the Newtonian fluid stress across the interface is given by equation (7) and $\boldsymbol{J}$ and $\boldsymbol{K}$ are known kernel functions. Hence,

$$-\int_{S_i}\left[\mathscr{C}_e^{-1}\boldsymbol{n}\nabla_s\cdot\boldsymbol{n} - [\![\boldsymbol{n}\cdot\boldsymbol{T}^E]\!]\right]\cdot\boldsymbol{J}\,\mathrm{d}S_y - (1-\lambda)\int_{S_i}\boldsymbol{n}\cdot\boldsymbol{K}\cdot\boldsymbol{u}\,\mathrm{d}S_y$$

$$= \begin{cases}\boldsymbol{u}(\boldsymbol{x}), & \boldsymbol{x}\in V, \quad (18a)\\ \dfrac{1+\lambda}{2}\boldsymbol{u}(\boldsymbol{x}_s), & \boldsymbol{x}_s\in S_i, \quad (18b)\\ \lambda\bar{\boldsymbol{u}}(\boldsymbol{x}), & \boldsymbol{x}\in\bar{V}, \quad (18c)\end{cases}$$

which is an integral equation of the second kind that may be solved for the interfacial velocity $\boldsymbol{u}(\boldsymbol{x}_s)$. The drop shape evolves according to

$$\frac{\mathrm{d}\boldsymbol{x}_s}{\mathrm{d}t} = \boldsymbol{u}(\boldsymbol{x}_s), \quad (19)$$

though it is frequently best from the standpoint of a numerical implementation to evolve marker points, which are distributed along the boundary, by moving with the local normal component of velocity only.

The standard numerical approach for this free-boundary problem is to first solve equation (16) to obtain the normal component of the electric field, then determine the tangential component E_t according to (15). After calculating the electrical stress from (4) and evaluating the curvature $\nabla_s\cdot\boldsymbol{n}$ for the given shape S_i, the interfacial velocity calculated from (18) and (19) is used to step the shape forward in time using a simple Euler method. The calculation is repeated sequentially for each shape generated.

2.5. *Numerical implementation*

In this paper we are only concerned with axisymmetric two-drop configurations. In this case, as is well-known, the azimuthal part of the surface integrations in each of the integral equations can be performed analytically (e.g. Lee & Leal 1982; Sherwood 1988). N node points are distributed along the interface of each (identical) drop and, as a consequence of the symmetry, it is only necessary to determine the unknown values on one of the drops. Typically we chose $N = 61$; calculations with a larger number of points did not significantly change the results. The resulting equations are discretized by assuming that the unknown E_n and $\boldsymbol{u}$ distributions vary linearly

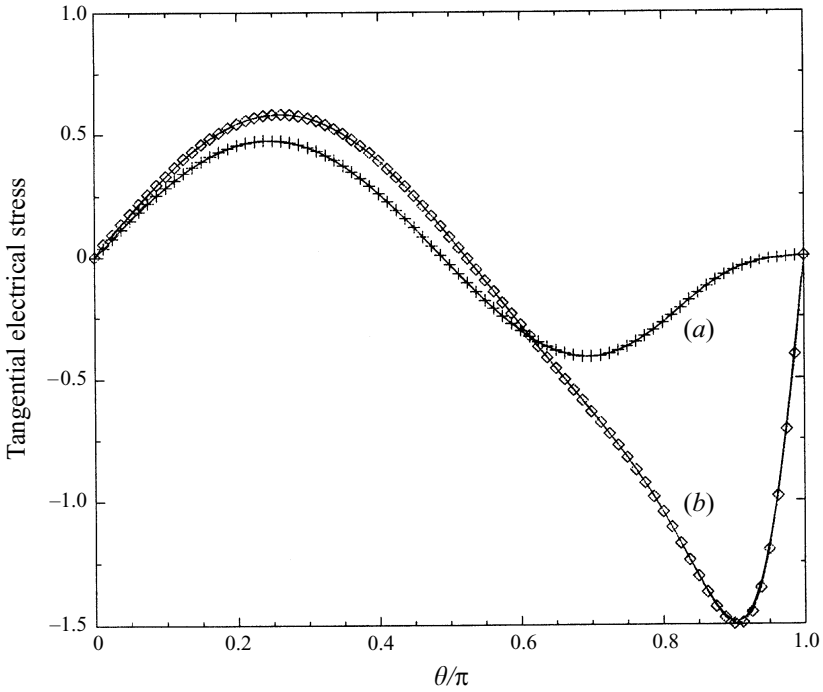

FIGURE 2. The tangential component of the electrical stress along the surface of one drop when two drops are placed in an electric field. A comparison of the numerical results (symbols) with the analytical results of Sozou (1975, figure 1) (solid curves). Centre-to-centre spacing is $2h = 2.2a$. (*a*) $\bar{\sigma}/\sigma = 0.05$, $\bar{\epsilon}/\epsilon = 1$; (*b*) $\bar{\sigma}/\sigma = 10$, $\bar{\epsilon}/\epsilon = 1$. θ is the usual polar angle measured from the positive z-axis.

between node points along the interface, after which the integral equations reduce to a linear system of equations that are solved numerically using standard IMSL routines. As $\boldsymbol{x}_s \rightarrow \boldsymbol{y}$ the integrands are singular, though integrable, and we subtract a small region about the singularity and perform the integration analytically. The free surface shape is represented using an arclength (s) description (e.g. Stone & Leal 1990), where the radial and axial node points, $r_i(s)$ and $z_i(s)$, are fitted with cubic splines. The normal and curvature along the surface are computed from these cubic spline representations. Integrations were performed in double precision using both four- and seven-point Gaussian quadrature routines, as well as the QUADPACK routine (DQAGS), and the results were essentially identical.

2.6. *Comparison with available analytical and numerical results*

We verified the numerical code by first evaluating the electric field, electric stresses, and velocity field for an isolated spherical drop placed in a uniform field. The numerical results were in excellent agreement with the theoretical predictions. Secondly, we compared the numerical results with available analytical results for two spherical drops (Sozou 1975). The largest fields and electrical stresses are generated for close separations. In figure 2 we show the agreement between the numerical calculations and Sozou's results for a centre-to-centre spacing $2h = 2.2a$ and two conductivity ratios, $\bar{\sigma}/\sigma = 10$ and $\bar{\sigma}/\sigma = 0.05$, for $\bar{\epsilon}/\epsilon = 1$. (Note that there are typographical errors in Sozou's equations (9) and (26).

The final check was to compare the deformations calculated with this numerical code with Sherwood's result (1988) for an isolated drop. The results were in good agreement (typically within a few percent), though Sherwood only reported cases where the distortions were prolate. In § 3 we also study cases where oblate distortions occur.

3. Numerical results

3.1. *Scaling arguments: electrical versus electrohydrodynamic interactions*

For the two-drop configuration, three qualitatively and quantitatively different interactions are possible that either substantially change the initial centre-of-mass separation distance or promote interface contact: (i) there is an electrically driven centre-of-mass motion owing to one drop appearing, to leading order, as a dipole in the far-field electrical disturbance produced by the second drop – this dielectrophoretic motion is always attractive and produces a relative velocity that scales proportional to $O(a/h)^4$; (ii) electrohydrodynamically driven centre-of-mass motion owing to a bulk fluid flow, caused by tangential electrical stresses at the surface of each drop, which, in turn, causes a nearby drop to translate with a velocity that scales proportional to $O(a/h)^2$ – this relative motion can be either attractive or repulsive depending on the sense of the circulation produced by the tangential electrical stresses; (iii) deformation-induced contact characteristic of low interfacial tensions (higher $\mathscr{C}_e$) and small separation distances. Note that mechanism (ii) does not arise for the perfect dielectric and/or perfectly conducting drops because, in such systems, tangential electrical stresses do not obtain unless the drops carry a native surface charge.

The electrically driven interactions of mechanism (i), on the other hand, are always present. Because each drop is electrically neutral, when exposed to a uniform electric field, a dipole response (equation (9*a*)) is produced with an electrical field that decays as $O(r^{-3})$. As is well-known in dielectrophoresis (Pohl 1978), a dipole at position $\boldsymbol{x}_1$, which has a strength proportional to the magnitude of the applied field $\boldsymbol{E}_\infty$, experiences a force proportional to $\boldsymbol{E}_\infty \cdot \nabla \boldsymbol{E}_\infty(\boldsymbol{x}_1, \boldsymbol{x}_2)$, where $\nabla \boldsymbol{E}_\infty(\boldsymbol{x}_1, \boldsymbol{x}_2)$ is the disturbance electric field gradient at $\boldsymbol{x}_1$ due to a drop positioned at $\boldsymbol{x}_2$ (Rivette & Baygents 1996). This force, with magnitude $O(\epsilon\epsilon_0 E_\infty^2 a^6/h^4)$ is balanced by viscous stresses on the translating drop and so, for two drops a distance $h = |\boldsymbol{x}_2 - \boldsymbol{x}_1|$ apart, the relative velocity U^T is

$$U^T = O\left(\frac{\epsilon\epsilon_0 E_\infty^2 a^5}{\mu h^4}\right). \tag{20}$$

On the other hand, electrohydrodynamic stresses at the drop interface produce a hydrodynamic dipolar far field which has a velocity that decays as $O(r^{-2})$ (equation (18*a*)). A neutrally buoyant drop translates at leading order with this local disturbance velocity and so moves with speed

$$U^T = O\left(\frac{\epsilon\epsilon_0 E_\infty^2 a^3}{\mu h^2}\right). \tag{21}$$

As shown below, these far-field arguments are, not surprisingly, in good agreement with the numerical calculations.

We now illustrate the typical kinds of interactions that we have observed in our numerical studies of two deformable drops. First, perfect dielectric drops are considered and, then, the interactions of two drops according to the leaky dielectric model are discussed.

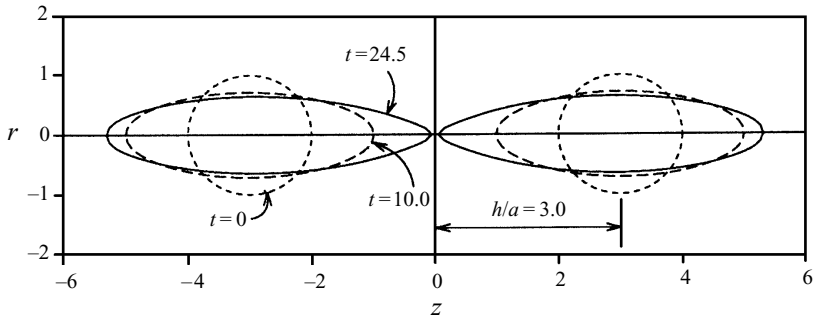

FIGURE 3. Deformation and approach of a pair of perfect dielectric drops; $\bar{\epsilon}/\epsilon = 8$, $\lambda = 1$, $\mathscr{C}_e = 1$. Initially $h = 3a$.

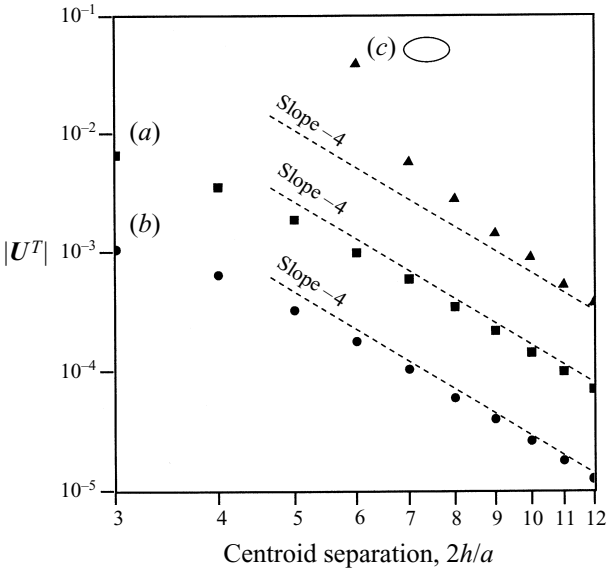

FIGURE 4. Drop velocity of perfect dielectric drops as a function of centroid (centre-to-centre) position. Dashed lines show the expected h^{-4} dependence of the electrically-driven centre-of-mass velocities. (*a*) $\bar{\epsilon}/\epsilon = 5$, $\lambda = 1$, $\mathscr{C}_e = 0.1$, 1% maximum deformation; (*b*) $\bar{\epsilon}/\epsilon = 0.4$, $\lambda = 1$, $\mathscr{C}_e = 1$, 5% maximum deformation; (*c*) $\bar{\epsilon}/\epsilon = 8$, $\lambda = 1$, $\mathscr{C}_e = 1$, 57% maximum deformation.

3.2. *Perfect dielectric drop pairs*

We begin in figure 3 with a typical interaction of two initially spherical perfect dielectric drops with $\bar{\epsilon}/\epsilon = 8, \mathscr{C}_e = 1$ and $\lambda = 1$. With an initial separation of $2h = 6a$, the drops first deform into prolate ellipsoidal shapes, which would have an aspect ratio $L/B = 3.65$ if the drops were instead isolated in a uniform electric field. The drops subsequently translate toward one another, which thereby increases the disturbance electric field causing enhanced prolate distortions of the drops, and, in particular, substantial deformation in the near contact region. Indeed, the interfaces in the gap region neck toward one another until the simulation is stopped just before contact.

In order to study the electrically driven interaction (or perhaps it would be better to say dielectrophoretically driven interaction), we show in figure 4 the velocity of the centre of mass as a function of the dimensionless separation distance $2h/a$ for three different ratios of dielectric constants; the capillary numbers are small enough

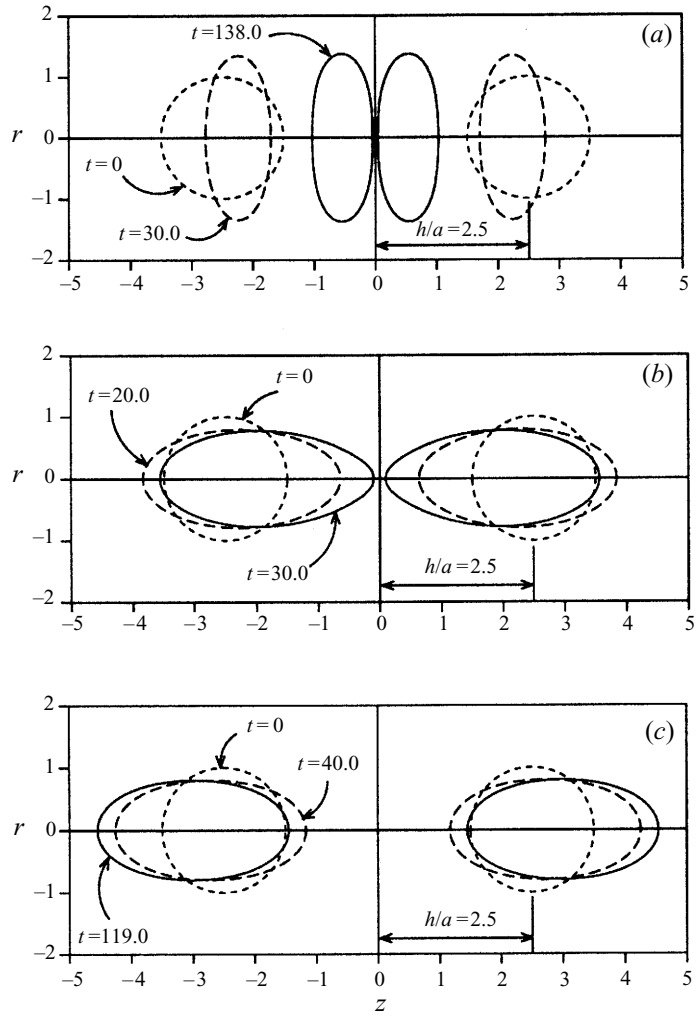

FIGURE 5. Three types of behaviour characteristic of drop deformation and interaction in the leaky dielectric model: (*a*) drops deform oblately and come together; $\bar{\sigma}/\sigma = 2, \bar{\epsilon}/\epsilon = 8$, $\lambda = 1$, $\mathscr{C}_e = 1$; (*b*) drops deform prolately and come together; $\bar{\sigma}/\sigma = 6, \bar{\epsilon}/\epsilon = 8$, $\lambda = 1$, $\mathscr{C}_e = 1.5$; (*c*) drops deform prolately and move apart; $\bar{\sigma}/\sigma = 1.04, \bar{\epsilon}/\epsilon = 0.2$, $\lambda = 1$, $\mathscr{C}_e = 1.5$.

that distortions are modest. The numerical results are in good agreement with the asymptotic prediction $U^T \propto h^{-4}$ discussed in § 3.1. When distortions are large the numerical results deviate noticeably from the h^{-4} scaling when $h < 4a$ (figure 4, case *c*). On the other hand, when distortions are smaller, the h^{-4}, scaling for the centre-of-mass velocity holds for separations as small as $h \approx 2a - 3a$.

For perfect dielectric drops the electrical stresses always act normal to the drop surface (Melcher & Taylor 1969; Sherwood 1988), which limits the range of behaviour observed: the drops always deform prolately and are always drawn together by electrical interactions. The only qualitative variations occur as the deformation is varied. When $D \ll 1$, the close approach of the drops is resisted by lubrication forces. An indication of this effect can be seen in figure 4 where the rate of change of velocity with separation distance decreases for the perfect dielectrics with small

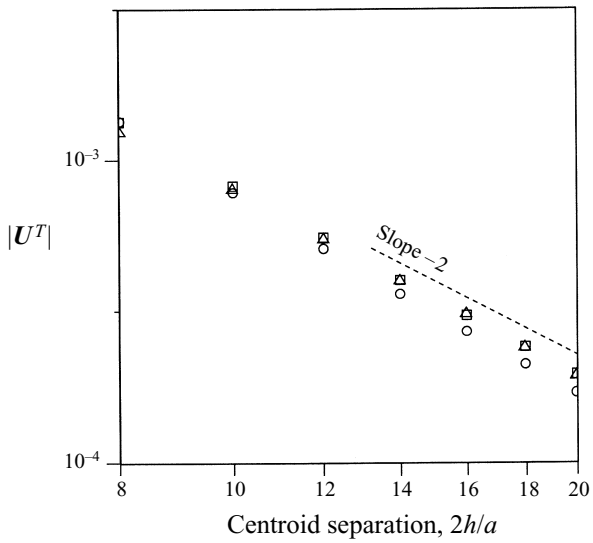

FIGURE 6. Drop velocity of leaky dielectric drops as a function of centroid (centre-to-centre) position. Dashed lines show the expected $(h/a)^{-4}$ dependence of the electrically-driven centre-of-mass velocities. ○, $\bar{\sigma}/\sigma = 4, \bar{\epsilon}/\epsilon = 8$, $\lambda = 1$, $\mathscr{C}_e = 1$, 7% maximum deformation; □, $\bar{\sigma}/\sigma = 5, \bar{\epsilon}/\epsilon = 8$, $\lambda = 1$, $\mathscr{C}_e = 1$, 6% maximum deformation; △, $\bar{\sigma}/\sigma = 1.04, \bar{\epsilon}/\epsilon = 0.2$, $\lambda = 1$, $\mathscr{C}_e = 0.1$, 2% maximum deformation.

deformations even though the electrical interactions, which drive the translation, become progressively stronger. For $D = O(1)$, the drop surface is more compliant, and so as the separation between the drops diminishes, the electrical interactions give rise to field-enhanced deformation and the drop surfaces are pulled together with little resistance by viscous stresses. Thus, in figure 4, case *c* the numerical results for a very deformable perfect dielectric drop illustrate a substantially increasing velocity as the centroid separation decreases.

3.3. *Leaky dielectric drop pairs*

Leaky dielectric drops exhibit a much richer variety of microstructural responses to the imposition of the electric field. As shown in figure 5, for a fixed initial separation $2h = 5a$, three classes of behaviour are observed depending on the ratios $\bar{\sigma}/\sigma$ and $\bar{\epsilon}/\epsilon$: the drops first deform oblately – that is, they stretch orthogonal to the axis of symmetry – and then translate together (figure 5*a*); the drops deform prolately and translate together (figure 5*b*); or the drops deform prolately and move apart (figure 5*c*). These classes of behaviour are generally observed provided that h/a is sufficiently large, and $\mathscr{C}_e$ sufficiently small, to ensure that the drop surfaces are not brought into close proximity simply as a result of interface deformation.

These different responses occur because of tangential electrical stresses that result from conduction processes. The fluid motion produced by these interfacial stresses decays as r^{-2} and so is much stronger than the typical dielectrophoretic translational motion. The sense of the circulation depends on the sign of the quantity $\bar{\sigma}/\sigma - \bar{\epsilon}/\epsilon$ and so determines whether the fluid motion brings the two drops together or pushes them apart. If $\bar{\sigma}/\sigma < \bar{\epsilon}/\epsilon$, the electrically driven circulation about one drop pulls the second drop closer, as in figures 5(*a*) and 5(*b*); if $\bar{\sigma}/\sigma > \bar{\epsilon}/\epsilon$, the sense of the circulation changes and the flow pushes the second drop away, as in figure 5(*c*). Irrespective of the sign of $(\bar{\sigma}/\sigma - \bar{\epsilon}/\epsilon)$, the drop velocities will vary as $(h/a)^{-2}$ for $h/a \gg 1$. This scaling

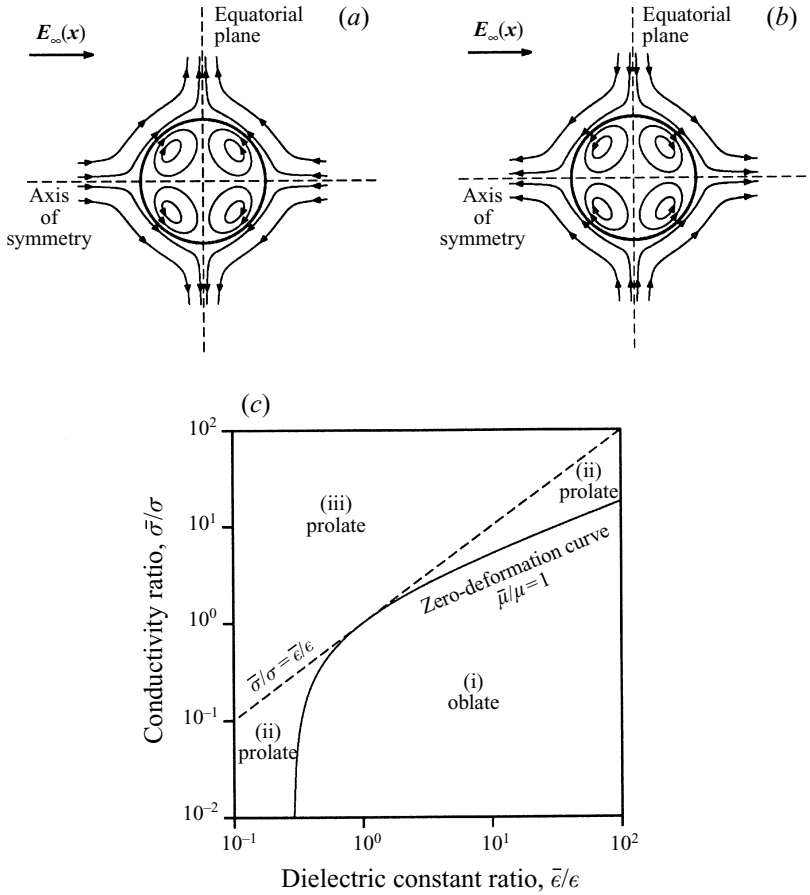

FIGURE 7. (*a*, *b*) Qualitative circulation patterns according to the leaky dielectric model for an isolated drop in a uniform electric field and (*c*) a map of the expected shape response, which has a significant influence on the interaction, as a function of the conductivity and dielectric constant ratios. (*a*) $\bar{\sigma}/\sigma < \bar{\epsilon}/\epsilon$: flow is drawn in along the axis of symmetry and expelled in the equatorial plane; (*b*) $\bar{\sigma}/\sigma > \bar{\epsilon}/\epsilon$: flow is drawn in from the equatorial plane and expelled along the axis of symmetry. (*c*) The zero deformation curve, equation (14), and the line for perfect dielectric, $\bar{\sigma}/\sigma = \bar{\epsilon}/\epsilon$, delineate three combinations of deformation and circulation: (i) oblate deformation and circulation as in (*a*); (ii) prolate deformation and circulation as in (*a*); (iii) prolate deformation and circulation as in (b).

is documented in figure 6, which reports the numerically determined centre-of-mass velocities for nearly spherical drops as a function of the separation distance for three different sets of conductivity and dielectric constant ratios.

The qualitative features of the three types of responses described above for the drop-pair interactions can be understood by constructing a map of the $(\bar{\sigma}/\sigma, \bar{\epsilon}/\epsilon)$ parameter space as shown in figure 7. As discussed earlier (equation (14)), a discriminating function $f_d(\bar{\sigma}/\sigma, \bar{\epsilon}/\epsilon, \lambda)$ distinguishes conditions giving rise to oblate or prolate drop shapes. The discriminating function is a weak function of λ and is plotted in figure 7 for $\lambda = 1$. Also, included in figure 7 is the $\bar{\sigma}/\sigma = \bar{\epsilon}/\epsilon$ line, which distinguishes electrically driven circulation patterns (see figure 7*a*, *b*) that are attractive from those that are repulsive. This 'map' of property values thus makes it easy to predict the approximate shape of the drops, at least for sufficiently large separation distances.

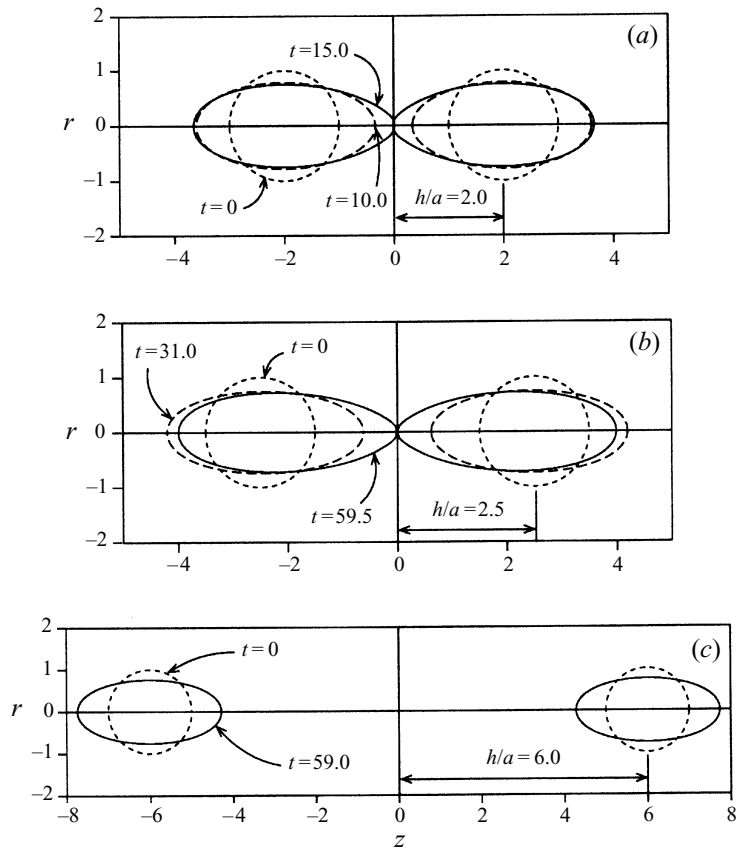

FIGURE 8. Drop deformation and translation as a function of the initial separation distance h/a; $\bar{\sigma}/\sigma = 5, \bar{\epsilon}/\epsilon = 4$, $\lambda = 1$, and $\mathscr{C} = 1$. (*a*) Initial centre-to-centre separation distance is 4 radii and the drops touch owing to deformation; (*b*) initial centre-to-centre separation distance is 5 radii and the drops translate together owing to dielectrophoretic interactions; (*c*) initial centre-to-centre separation distance is 12 radii and the drops deform and drift apart slowly owing to the induced circulatory flows which are repulsive in character.

Hence, it is reasonably straightforward to characterize conditions leading to oblate drop shapes that translate together, prolate drop shapes that translate together, and prolate drop shapes that translate apart.

However, it is important to note that *not all* of the qualitative features of the electrically driven microstructural response of the drop pair can be deduced from the far-field properties of equations (9) and (18) or, equivalently, from figure 7(*c*). To illustrate this point we show in figure 8 numerical simulations of the drop shape varying the initial separation distance with $\mathscr{C}_e = 1$, $\bar{\sigma}/\sigma = 5$ and $\bar{\epsilon}/\epsilon = 4$, from which far-field considerations would lead one to expect prolate deformations that drift apart. The associated centre-of-mass velocity as a function of separation distance is shown in figure 9. In this case, we find that sufficiently large initial separations are dominated by the electrohydrodynamic response; for smaller separation distances, though, the drops drift and deform together. In particular, since $\bar{\sigma}/\sigma > \bar{\epsilon}/\epsilon$, the hydrodynamic interactions are repulsive and, for separations in excess of approximately 9.8, the drops indeed move apart, although they do so slowly and the velocity only goes over to the $(h/a)^{-2}$ scaling slowly. However, when $h/a < 9.8$, the drops translate toward

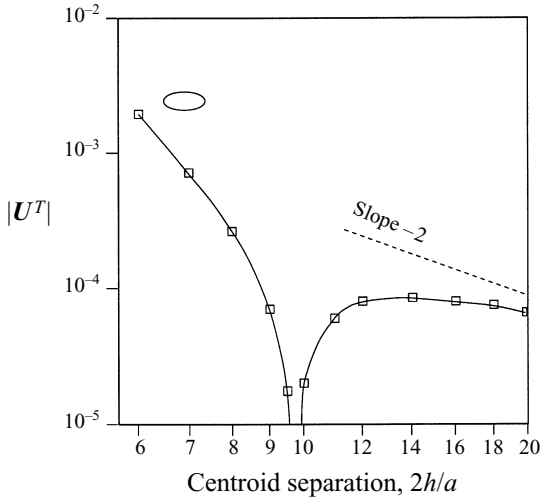

FIGURE 9. Centre-of-mass velocity versus separation distance; $\bar{\sigma}/\sigma = 5, \bar{\epsilon}/\epsilon = 4$, $\lambda = 1$, $\mathscr{C}_e = 1$.

each other as a result of significant electrical interactions. In this case, the attractive electrical interactions can more than counterbalance the influence of the circulation patterns.

4. Conclusions

We have presented a numerical investigation of the interaction of two drops in a uniform electric field. The leaky dielectric model is used to describe the electrical influences of the fluid. In particular, conduction processes produce viscous stresses that are capable of deforming isolated drops, as is well known. Here we also observed the effect of circulatory flows, driven by electrohydrodynamic stresses, on the motion of the drop pairs. Whereas dielectrophoresis of the two drops always leads to attractive interactions, electrohydrodynamic stresses may cause sufficiently widely spaced drops to be pushed apart. Scaling estimates for the relative translation speed of the drops are in good agreement with the numerical simulations when either dielectrophoretic motions or electrodynamic flows dominate.

In closing we compare the strength of the electrohydrodynamic flows to electrophoretic motion of the drops, which would result from a native surface charge density q. An electrokinetic velocity scale is $qE_\infty/\kappa\mu$, where κ is the Debye screening parameter. The strength of the electrokinetic motion relative to the electrohydrodynamics is given by $q/a\kappa\epsilon\epsilon_0 E_\infty$, provided the viscosity of the drops does not greatly exceed that of the surrounding fluid. In poorly conducting media, surface charge densities and Debye screening parameters tend to be small, due to the low dielectric constant of the fluids (Kuo & Osterle 1967; Stotz 1978; Ehrlich & Melcher 1982). Additionally, applied field strengths can be appreciable, i.e. $O(10^5\ \mathrm{V\ m^{-1}})$ and higher. Using the characteristic values $q = 10^{-6}\ \mathrm{C\ m^{-2}}$, $\kappa = 10^6\ \mathrm{m^{-1}}$ and $\epsilon = 3$, one finds that $q/a\kappa\epsilon\epsilon_0 E_\infty$ is approximately 4×10^{-5} for a cm-sized drop. Thus, except at the larger separations, relative motion of the drops appears to be dominanted by electrohydrodynamics. Of course under different circumstances (e.g. smaller drops, lower field strengths, aqueous media, etc.), electrokinetic effects are significant and presumably cannot be ignored.

The authors are grateful to NASA (grant NAG8-948) for support of this research. H. A. S. thanks J. D. Sherwood for many helpful conversations.

REFERENCES

Allan, R. S. & Mason, S. G. 1962 Particle behaviour in shear and electric fields: I. Deformation and burst of fluid drops. *Proc. R. Soc. Lond.* A **267**, 45–61.

Arp, P. A., Foister, R. T. & Mason, S. G. 1980 Some electrohydrodynamic effects in fluid dispersions. *Adv. Colloid Interface Sci.* **12**, 295–356.

Baygents, J. C. & Saville, D. A. 1989 The circulation produced in a drop by an electric field: A high field strength electrokinetic model. *AIP Conf. Proc. 197, Third Intl Colloquium on Drops and Bubbles*, pp. 7–17.

Baygents, J. C. & Saville, D. A. 1991*a* Electrophoresis of drops and bubbles. *J. Chem. Soc. Faraday Trans.* **87**, 1883–1898.

Baygents, J. C. & Saville, D. A. 1991*b* Electrophoresis of small particles and fluid globules in weak electrolytes. *J. Colloid Interface Sci.* **146**, 9–37.

Brazier-Smith, P. R. 1971 Stability and shape of isolated and pairs of water drops in an electric field. *Phys. Fluids* **14**, 1–6.

Brazier-Smith, P. R., Jennings, S. G. & Latham, J. 1971 An investigation of the behaviour of drops and drop-pairs subjected to strong electrical forces. *Proc. R. Soc. Lond* A **325**, 363–376.

Brooks, D. E., Sharp, K. A., Bamberger, S., Tamblyn, C. H., Seaman, G. V. F. & Walter, H. 1984 Electrostatic and electrokinetic potentials in two polymer aqueous phase systems. *J. Colloid Interface Sci.* **102**, 1–13.

Byers, C. H. & Amarnath, A. 1995 Understand the potential of electro-separations. *Chem. Engng. Prog.* **91**, 63–69.

Ehrlich, R. M. & Melcher, J. R. 1982 Bipolar model for traveling-wave induced nonequilibrium double-layer streaming in insulating liquids. *Phys. Fluids* **25**, 1785–1793.

Harris, M. T. & Basaran, O. A. 1993 Capillary electrohydrostatics of conducting drops hanging from a nozzle in an electric field. *J. Colloid Interface Sci.* **161**, 389–413.

Kuo, S. & Osterle, F. 1967 High field electrophoresis in low conductivity liquids. *J. Colloid Interface Sci.* **25**, 421–428.

Latham, J. & Roxburgh I. W. 1966 Disintegration of pairs of water drops in electric fields. *Proc. R. Soc. Lond* A **295**, 84–97.

Lee, S. H. & Leal, L. G. 1982 The motion of a sphere in the presence of a deformable interface. II. A numerical study of the translation of a sphere normal to an interface. *J. Colloid Interface Sci.* **87**, 81–106.

Li, H., Halsey, T. & Lobkovsky, A. 1994 Singular shape of a fluid drop in an electric or magnetic field. *Europhys. Lett.* **27**, 575–580.

Melcher, J. R. 1973 Electrohydrodynamics. *Proc. IUTAM 13th Intl Congr. Theor. Appl. Mech., Moscow Univ. 1972* (ed. E. Becker & G. K. Mikhailov), pp. 240–63.

Melcher, J. R. & Taylor, G. I. 1969 Electrohydrodynamics: A review of the role of interfacial shear stresses. *Ann. Rev. Fluid Mech.* **1**, 111–146.

Miksis, M. J. 1981 Shape of a drop in an electric field. *Phys. Fluids* **24**, 1967–1972.

Pohl, H. A. 1978 *Dielectrophoresis.* Cambridge University Press.

Pozrikidis, C. 1992 *Boundary Integral and Singularity Methods for Linearized Viscous Flow*. Cambridge University Press.

Ptasinski, K. J. & Kerkhof, P. J. A. M. 1992 Electric field driven separations: phenomena and applications. *Sep. Sci. Tech.* **27**, 995–1021.

Rallison, J. M. & Acrivos, A. 1978 A numerical study of the deformation and burst of a viscous drop in an extensional flow. *J. Fluid Mech.* **89**, 191–200.

Rivette, N. J. & Baygents, J. C. 1996 A note on the electrostatic force and torque acting on an isolated body in an electric field. *Chem. Engng Sci.* **51**, 5205–5211.

Scott, T. C. 1989 Use of electric fields in solvent extraction: A review and prospectus. *Sep. Purif. Meth.* **18**, 65–109.

Sherwood, J. D. 1988 Breakup of fluid droplets in electric and magnetic fields. *J. Fluid Mech.* **188**, 133–146.

Sherwood, J. D. 1991 The deformation of a fluid drop in an electric field: a slender-body analysis. *J. Phys.* A: *Math. Gen.* **24**, 4047–4053.

Sozou, C. 1975 Electrohydrodynamics of a pair of liquid drops. *J. Fluid Mech.* **91**, 541–546.

Stone, H. A. & Leal, L. G. 1990 The effects of surfactants on drop deformation and breakup. *J. Fluid Mech.* **220**, 161–186.

Stone, H. A., Lister, J. R. & Brenner, M. P. 1998 Drops with conical ends in electric and magnetic fields. Submitted to *Proc. R. Soc. Lond.*

Stotz, S. 1978 Field dependence of the electrophoretic mobility of particles suspended in low-conductivity liquids. *J. Colloid Interface Sci.* **65**, 118–130.

Tanzosh, J., Manga, M. & Stone, H. A. 1992 Boundary integral methods for viscous free-boundary problems: Deformation of single and multiple fluid-fluid interfaces. *Proc. Boundary Element Technologies VII.* (ed. C. A. Brebbia & M. S. Ingber), pp. 19–39. Computational Mechanics Publications.

Taylor, G. I. 1964 Disintegration of water drops in electric fields. *Proc. R. Soc. Lond.* A **280**, 383–397.

Taylor, G. I. 1966 Studies in electrohydrodynamics: I. The circulation produced in a drop by an electric field. *Proc. R. Soc. Lond.* A **291**, 159–166.

Taylor, G. I. 1968 The coalescence of closely spaced drops when they are at different electric potentials. *Proc. R. Soc. Lond.* A **306**, 423–434.

Torza, S., Cox, R. G. & Mason, S. G. 1971 Electrohydrodynamic deformation and burst of liquid drops. *Phil. Trans. R. Soc. Lond.* A **269**, 295–319.

Vizika, O. & Saville, D. A. 1992 The electrohydrodynamic deformation of drops suspended in liquids in steady and oscillatory electric fields. *J. Fluid Mech.* **239**, 1–21.

Zhang, X., Basaran, O. A. & Wham, R. M. 1995 Theoretical prediction of electric field-enhanced coalescence of spherical drops. *AIChE J.* **41**, 1629–1639.